

**The S52F FOXF1 Mutation Inhibits STAT3 Signaling and Causes Alveolar Capillary
Dysplasia**

Arun Pradhan^{1,2}, Andrew Dunn^{1,7}, Vladimir Ustiyan^{1,2}, Craig Bolte^{1,2}, Guolun Wang^{1,2}, Jeffrey A. Whitsett², Yufang Zhang^{1,2}, Alexey Porollo³, Yueh-Chiang Hu⁴, Rui Xiao^{5,6}, Przemyslaw Szafranski⁶, Donglu Shi⁷, Pawel Stankiewicz⁶, Tanya V. Kalin², and Vladimir V. Kalinichenko^{1,2}

Online supplementary methods

Generation of *Foxf1*^{WT/S52F} mouse line

Foxf1^{WT/S52F} line was generated in the Genome Editing Core of the Cincinnati Children's Hospital Research Foundation using CRISPR/Cas9 editing. Multiple sgRNAs that target around the intended mutation site were selected, according to the off-target scores from the CRISPR Design Tool website (<http://www.genome-engineering.org/>). sgRNA vector construction were described previously (E1). Briefly, pairs of complementary DNA oligos with compatible overhangs were annealed and cloned into a pX458 vector that carries a U6 promoter to drive sgRNA expression and a ubiquitously expressed promoter to drive *Cas9*-2A-GFP expression (Addgene plasmid #43138). sgRNA editing activity was evaluated in mouse mK4 cells by the T7E1 assay (New England Biolabs), and compared side-by-side with *Tet2* sgRNA that has been shown to edit the mouse genome efficiently (E2). Validated sgRNA and *Cas9* mRNA were *in vitro* transcribed using MEGAshorscript T7 kit and mMESSAGING mMACHINE T7 ULTRA kit (Thermo Fisher), respectively, according to manufacturer's instruction. The single-stranded donor oligo that carries homologous arms (>55 nt each end) and intended mutations with additional silent mutations to create new restriction enzyme sites was subsequently designed. sgRNA, *Cas9* mRNA, and donor ssDNA were mixed at concentration of 50, 100, and 100 ng/ul, respectively, and injected to the cytoplasm of one-cell-stage embryos of B6D2F2 genetic background. Injected embryos were immediately transferred into the oviductal ampulla of pseudopregnant CD-1 females. Live born pups were genotyped by PCR using primers provided in Table E1. Genotypes were confirmed by Sanger sequencing. Mice were bred and housed in a vivarium with a 12-hour light/dark cycle.

Luciferase assay

The LUC plasmid containing 6X FOXF1 binding sites (E3) was co-transfected with *CMV-WT-FOXF1* (or its mutants) expression vectors in HEK293T cells using Lipofectamine (Invitrogen). *CMV-empty* vector was used as a control. In addition, *CMV-Renilla* was used as an internal control to normalize the transfection efficiency. A dual-luciferase assay (Promega) was performed 48 h after transfection (E4-E6).

Immunofluorescence microscopy was performed and the images were obtained using a Zeiss Axioplan 2 Imaging Universal Microscope with an Axiocam MRm digital camera (Axiovision Release 4.3) as described (E7, E8).

Immunohistochemistry and immunofluorescence

Paraffin sections were stained with hematoxylin and eosin (H&E) or with following Abs: PECAM1 (Abcam), STAT3 (Cell signaling Technology), pSTAT3 (Cell signaling Technology), FLK1 (Santa Cruz Biotechnology), Ki-67 (ThermoFisher Scientific) and CCND1 (Abcam). For co-localization experiments, secondary antibodies conjugated with Alexa Fluor 488 or Alexa Fluor 594 (Invitrogen) were used.

siRNA transfection

To decrease FOXF1 levels, we used siRNAs targeting either ORF (Mouse: 5'-GAAAGGAGUUUGUCUUCUC-3') or 3'UTR (Mouse: 5'-CCAGAUACGUGGAAAGAAUUU-3') (Dharmacon) using LipofectamineTM 2000 reagent (Invitrogen) (E9). For STAT3 knockdown siStat3-1 (Mouse: 5'-AGUGAGUGUGGGUGAUAAAUU---3') and siStat3-2 (Mouse; 5'---ACAUAGAAGCUAGGACUAAUU-3') were used. Cells were harvested 48 hours after transfection and used for immunoblot analysis.

Chip-seq

ChIP-Seq library was prepared using Chipmentation procedure and libraries were sequenced using Illumina HiSeq 2500 at CCHMC sequencing core. Data analysis was performed using the BioWardrobe platform. FOXF1 ChIPseq data (GEO Accession GSE100149) was aligned with STAT3 ChIPseq (GEO Accession GSM2300474) ChIPseq data for histone methylation (GEO Accession GSE31039) using the BioWardrobe platform.

Preparation of nanoparticles

Methoxypolyethylene glycol amine Mn = 2000 (PEG_{NH2}) was obtained from Nanocs. Polyethylenimine (Mn = 600), Myristic Acid (MA) ≥ 99%, Oleic Acid (OA ≥ 99%), Cholesterol (BioReagent ≥ 99%), Ethanol (EtOH, 200p), HPLC grade water, 2-(N-morpholino)ethanesulfonic acid (MES) ≥ 99% and 3-(N-Morpholino)propanesulfonic acid (MOPS) were obtained through Sigma-Aldrich and used without further purification. 1-ethyl-3-(3-dimethylaminopropyl)carbodiimide hydrochloride (EDC), N-hydroxysuccinimide (NHS), DyLight 650 NHS Ester, and Spectrum™ Spectra/Por™ 3.5 kDa Slide-A-Lyzer™ were obtained through ThermoFisher Scientific. Diethyl ether (anhydrous, BHT stabilized), and 20 kDa MWCO dialysis tubing were obtained through Fisher Scientific.

Functionalization of PEI with biological fatty acids and PEG was completed through amidation using EDC/NHS mediated coupling in 95% ethanol buffered with 25 mM MES, pH = 6. Carboxylate groups were reacted by EDC/NHS for 15 minutes at 40 °C. PEI or PEG_{NH2} was quickly added following carboxylate group activation and was allowed to react overnight at 40 °C to create PEI₆₀₀-MA₅ or PEG-OA. Ethanol was removed by rotary evaporation, the polymer resuspended in water, and dialyzed against water using a 20 kDa membrane for 4-5 days.

Colloids were then extracted twice in diethyl ether and lyophilized. Cholesterol was dissolved in ethanol. Lyophilized polymers were suspended in 10 mM MOPS, pH =7.4. PEI₆₀₀-MA₅ was stabilized with cholesterol and PEG-OA through solvent diffusion and microfluidic mixing at a mass ratio of 85:15:10, PEI:Cholesterol:PEG. PEI₆₀₀-MA₅ was conjugated with DyLight 650 overnight at room temperature in 10 mM MOPS. Residual ethanol was removed by dialysis against an isotonic dextran solution using a 3.5 kDa Slide-A-Lyzer™. Intravenous injections were performed using colloids mixed with plasmids at a mass ratio (w/w) of 24 in normal glucose. 5 µg plasmids in 20 µl were used for intravenous injections in neonatal mice. Infrared spectroscopy was run on a Nicolet attenuated total reflection Fourier transform infrared (ATR-FTIR) spectrometer outfitted with a diamond crystal. Hydrodynamic size and zeta potential were measured on a Malvern Zetasizer Nano ZS in normal glucose. In PEI/PEG nanoparticles, lipidic composition of the membrane influences the size and zeta potential of the polymer colloids that affect the efficiency of endothelial targeting.

References:

- E1. Ran FA, Hsu PD, Wright J, Agarwala V, Scott DA, Zhang F. Genome engineering using the CRISPR-Cas9 system. *Nat Protoc* 2013; 8: 2281-2308.
- E2. Wang H, Yang H, Shivalila CS, Dawlaty MM, Cheng AW, Zhang F, *et al.* One-step generation of mice carrying mutations in multiple genes by CRISPR/Cas-mediated genome engineering. *Cell* 2013; 153: 910-918.
- E3. Kim IM, Zhou Y, Ramakrishna S, Hughes DE, Solway J, Costa RH, *et al.* Functional characterization of evolutionarily conserved DNA regions in forkhead box f1 gene locus. *J Biol Chem* 2005; 280: 37908-16.

- E4. Cheng XH, Black M, Ustiyanyan V, Le T, Fulford L, Sridharan A, *et al.* SPDEF inhibits prostate carcinogenesis by disrupting a positive feedback loop in regulation of the Foxm1 oncogene. *PLoS Genet* 2014; 10: e1004656.
- E5. Balli D, Ren X, Chou FS, Cross E, Zhang Y, Kalinichenko VV, *et al.* Foxm1 transcription factor is required for macrophage migration during lung inflammation and tumor formation. *Oncogene* 2012; 31(34):3875-88.
- E6. Wang IC, Meliton L, Ren X, Zhang Y, Balli D, Snyder J, *et al.* Deletion of Forkhead Box M1 transcription factor from respiratory epithelial cells inhibits pulmonary tumorigenesis. *PLoS One* 2009; 4(8):e6609.
- E7. Sun L, Ren X, Wang IC, Pradhan A, Zhang Y, Flood HM, *et al.* The FOXM1 inhibitor RCM-1 suppresses goblet cell metaplasia and prevents IL-13 and STAT6 signaling in allergen-exposed mice. *Sci Signal* 2017; 10: eaai8583.
- E8. Ren X, Shah TA, Ustiyanyan V, Zhang Y, Shinn J, Chen G, *et al.* FOXM1 promotes allergen-induced goblet cell metaplasia and pulmonary inflammation. *Mol Cell Biol* 2013; 33(2):371-86.
- E9. Black M, Milewski D, Le T, Ren X, Xu Y, Kalinichenko VV, *et al.* FOXF1 Inhibits Pulmonary Fibrosis by Preventing CDH2-CDH11 Cadherin Switch in Myofibroblasts. *Cell Rep* 2018; 23(2):442-458.

Table E1: Primers for genotyping of S52F Foxf1 mice

Foxf1 +77/+94	<u>GGCGGCCAGGCCATGGAC</u>
Foxf1 +112/+133	<u>CACCAAGGCCAAGAAGACCAAC</u>
Foxf1 +334/+313	GATGAAGCACTCGTTGAGCGAC

Table E2: TaqMan primers for qRT-PCR reactions

Mouse TaqMan Gene expression assay	Catalogue No.
<i>Foxf1</i>	Mm00487497_m1
<i>Flk-1</i>	Mm01222421_m1
<i>Pecam1</i>	Mm01242584_m1
<i>Stat3</i>	Mm01219775_m1
<i>Bax</i>	Mm00432051_m1
<i>Ccnd1</i>	Mm00432359_m1
<i>Pdgfb</i>	Mm01298578_m1
<i>Mmp2</i>	Mm00439498_m1
<i>Mmp9</i>	Mm00442991_m1
<i>Actb</i>	Mm00607939_s1
<i>Acta2</i>	MM00725412_s1
<i>Pdpr</i>	Mm00494716_m1
<i>Sftpc</i>	Mm00488144_m1
<i>Scgb1a1</i>	Mm01230908_m1

Table E3: FACS antibodies

Antibody	Fluorophore	Clone	Company
CD16/32		93	eBioscience
CD31 (PECAM1)	eF405	390	eBioscience
CD326 (EpCAM)	PerCP-eF710	G8.8	eBioscience
CD45 (PTPRC)	eVolve605	30-F11	eBioscience

Table E4: Novel ACDMPV cases with *FOXF1* mutations.

Sequencing	Exon	cDNA	Protein	Inheritance	Interpretation	Pt survival	Additional anomalies	DNA source	Laboratory
FOXF1-S	1	c.145C>T	p.P49S	De novo	Likely pathogenic	N/A	N/A	Blood	BG
FOXF1-S	1	c.175A>G	p.M59V	Parents not tested	VUS	N/A	N/A	Blood	BG
FOXF1-S	1	c.178G>A	p.A60T	Parents not tested	VUS	N/A	N/A	Blood	BG
WES	1	c.191C>A	p.S64*	De novo	Pathogenic	N/A	N/A	Blood	BG
FOXF1-S	1	c.235C>T	p.Q79*	Not maternal	Pathogenic	11 days	N/A	Lung tissue	BG/Research
FOXF1-S	1	c.238_239delAG	p.S80Pfs*214	De novo	Pathogenic	12 days	CV, GI	Blood	Research
FOXF1-S	1	c.246C>G	p.F82L	De novo	Likely pathogenic	76 days	ACD without MPV	Blood	BG/Research
FOXF1-S	1	c.257G>C	p.R86P	De novo	Likely pathogenic	N/A	N/A	Blood	BG
FOXF1-S	1	c.266A>G	p.Y89C	De novo	Likely pathogenic	N/A	N/A	Blood	BG
FOXF1-S	1	c.267C>G	p.Y89*	Unknown	Pathogenic	N/A	N/A	N/A	BG
FOXF1-S	1	c.286G>A	p.V96M	De novo	Pathogenic	N/A	N/A	Blood	BG
FOXF1-S	1	c.286G>T	p.V96L	Parents not tested	Likely pathogenic	N/A	N/A	Blood	BG
FOXF1-S	1	c.289C>G	p.R97G	De novo	Likely pathogenic	N/A	N/A	Blood	BG
FOXF1-S	1	c.290G>A	p.R97H	De novo	Pathogenic	8 days	GI	Blood	Research
FOXF1-S	1	c.290G>A	p.R97H	De novo	Pathogenic	24 days	CV, GI	Lung tissue	BG/Research
FOXF1-S	1	c.302C>A	p.S101*	De novo	Pathogenic	N/A	N/A	N/A	BG
FOXF1-S	1	c.510C>G	p.Y170*	Unknown	Pathogenic	N/A	N/A	Buccal swab	BG
FOXF1-S	1	c.512G>C	p.G171A	Parents not tested	VUS	N/A	N/A	N/A	BG
FOXF1-S	1	c.614dupG	p.M206Hfs*89	De novo	Pathogenic	4 weeks	CV	Blood	Research
FOXF1-S	1	c.627delC	p.S210Afs*169	Unknown	Pathogenic	N/A	N/A	Blood	BG
FOXF1-S	1	c.691_698delGCGG CGGC	p.A231Rfs*61	Mosaic mother	Pathogenic	N/A	N/A	Blood	BG
FOXF1-S	1	c.802delG	p.A268Rfs*111	De novo	Pathogenic	2 weeks	N/A	Blood & lung tissue	Research
FOXF1-S	1	c.841_862del22	p.G281Sfs*91	Unknown	Pathogenic	12 days	CV, GI	Blood	BG/Research
FOXF1-S	1	c.849_850delTT	p.I285Qfs*9	Unknown	Pathogenic	2 weeks	CV, GI	Blood	BG/Research
FOXF1-S	1	c.852_856delTATCA	p.Y284*	Unknown	Pathogenic	N/A	N/A	Skin	BG
FOXF1-S	1	c.859C>T	p.Q287*	Unknown	Pathogenic	N/A	N/A	N/A	BG
FOXF1-S	1	c.965delC	p.P322Qfs*57	Unknown	Pathogenic	N/A	N/A	Blood	BG
FOXF1-S	2	c.1138T>A	p.*380Rext*73	Unknown	Pathogenic	N/A	N/A	Blood	BG

Abbreviations: BG, CLIA-certified Baylor Genetics laboratory; CV, cardiovascular; FOXF1-S, targeted Sanger sequencing; GI, Gastrointestinal WES, whole exome sequencing

None of these mutations was found in gnomAD <http://gnomad.broadinstitute.org/>

Table E5: Statistical analysis for figure 6C

<u>WT/ Vect vs S52F/ Vect</u>				<u>S52F/ Vect vs S52F/ STAT3</u>			
Targets	WT/ Vect	S52F/ Vect	<i>P-value</i>	Targets	S52F/ Vect	S52F/ STAT3	<i>P-value</i>
PDGF-β	1.0 ±0.19	0.55±0.11	0.0238	PDGF-β	0.55±0.11	1.59±0.19	0.0012
PECAM-1	1.0±0.21	0.45±0.18	0.0262	PECAM-1	0.45±0.18	1.7±0.17	0.0009
FLK-1	1.0±0.21	0.55±0.18	0.0479	FLK-1	0.55±0.18	2.1±0.17	0.0004
STAT3	1.0±0.15	0.25±.09	0.0018	STAT3	0.25±.09	2.13±.22	0.0002

<u>WT/ Vect vs WT/ STAT3</u>				<u>WT/ STAT3 vs S52F/ STAT3</u>			
Targets	WT/ Vect	WT/ STAT3	<i>P-value</i>	Targets	WT/ STAT3	S52F/ STAT3	<i>P-value</i>
PDGF-β	1.0 ±0.19	1.69±0.13	0.0066	PDGF-β	1.69±0.13	1.59±0.19	0.493
PECAM-1	1.0±0.21	1.9±0.18	0.0049	PECAM-1	1.9±0.18	1.7±0.17	0.234
FLK-1	1.0±0.21	2.0±0.19	0.0036	FLK-1	2.0±0.19	2.1±0.17	0.534
STAT3	1.0±0.15	2.3±0.2	0.0008	STAT3	2.3±0.2	2.13±.22	0.378

Table E6: Statistical analysis for figure 6D

WT/ Vect vs S52F/ Vect

Targets	WT/ Vect	S52F/ Vect	<i>P-value</i>
<i>Flk1</i>	5.81±1.35	2.44±1.44	0.0417
<i>Pecam1</i>	6.38±1.4	3.11±1.4	0.0459

S52F/ Vect vs S52F/ STAT3

Targets	S52F/ Vect	S52F/ STAT3	<i>P-value</i>
<i>Flk1</i>	2.44±1.44	8.66±1.88	0.0104
<i>Pecam1</i>	3.11±1.4	9.28±1.47	0.0062

WT/ Vect vs WT/ STAT3

Targets	WT/ Vect	WT/ STAT3	<i>P-value</i>
<i>Flk1</i>	5.81±1.35	9.24±1.4	0.0379
<i>Pecam1</i>	6.38±1.4	11.86±1.16	0.0064

WT/ STAT3 vs S52F/ STAT3

Targets	WT/ STAT3	S52F/ STAT3	<i>P-value</i>
<i>Flk1</i>	9.24±1.4	8.66±1.88	0.690
<i>Pecam1</i>	11.86±1.16	9.28±1.47	0.075

Table E7: Statistical analysis for endomucin area in figure 6G

<u>WT/ Vect vs S52F/ Vect</u>			<u>S52F/ Vect vs S52F/ STAT3</u>		
WT/ Vect	S52F/ Vect	<i>P-value</i>	S52F/ Vect	S52F/ STAT3	<i>P-value</i>
15.384±1.18	7.450±2.25	0.0001	7.450±2.25	15.382±2.03	0.0001

<u>WT/ Vect vs WT/ STAT3</u>			<u>WT/ STAT3 vs S52F/ STAT3</u>		
WT/ Vect	WT/ STAT3	<i>P-value</i>	WT/ STAT3	S52F/ STAT3	<i>P-value</i>
15.384±1.18	15.934±2.02	0.4674	15.943±2.02	15.382±2.03	0.5508

Table E8: Statistical analysis for figure 6F

<u>WT/ Vect vs S52F/ Vect</u>				<u>S52F/ Vect vs S52F/ STAT3</u>			
	WT/ Vect	S52F/ Vect	<i>P-value</i>		S52F/ Vect	S52F/ STAT3	<i>P-value</i>
Ki67	64.13±5.21	15.68±5.66	0.0004	Ki67	15.68±5.66	55.81±7.69	0.0019

<u>WT/ Vect vs WT/ STAT3</u>				<u>WT/ STAT3 vs S52F/ STAT3</u>			
	WT/ Vect	WT/ STAT3	<i>P-value</i>		WT/ STAT3	S52F/ STAT3	<i>P-value</i>
Ki67	64.13±5.21	67.88±6.62	0.4837	Ki67	67.88±6.62	55.81±7.69	0.1084

E1-E20 Figure legends

Figure E1. **A summary of *FOXF1* point mutations in human ACDMPV.** Forkhead box DNA binding, cell-type specific activation, and general activation domains of FOXF1 are shown as blue, green, and pink rectangles, respectively. Locations of mutations are shown with lines and details of the mutations are shown next to them. Yellow lines depict nonsense point mutations, whereas purple, blue, and green indicate missense, frameshift, and indel mutations, respectively. Novel mutations are represented in red. Previously reported mutations are represented in black.

Figure E2. **FOXF1 interacts with STAT3 protein.** (A-B) The PPYSY region of FOXF1 is conserved. Sequences show the alignment of the P49-Y53 (PPYSY) FOXF1 region amongst several species and between different members of Forkhead box family proteins. (C) Immunoblots show the FOXF1-STAT3 interaction in IP from total lung extracts. WT mice were treated with butylated hydroxytoluene (BHT) for 6 days to induce lung injury. (D) Immunoblots show the overlapping co-fractionation profiles of FOXF1 and STAT3 using a superose-6 gel filtration column.

Figure E3. **Y284A, Y284A/I285Q and S291* FOXF1 mutations do not disrupt FOXF1-STAT3 protein-protein interactions.** (A-B) Expression of HF-tagged FOXF1 proteins in MFLM-91U fetal lung endothelial cells. HF-tagged FOXF1 or its mutants were stably transfected into MFLM-91U cells. Western blot was used to visualize transfected proteins and β -actin. (C-D) Immunoblots show that transfected FOXF1 mutant proteins interact with STAT3. FOXF1-STAT3 interactions were detected after transfection of Y284A, Y284A/I285Q and S291* *Foxfl* constructs. Exogenous HF-FOXF1 mutant proteins were detected by α -Flag antibody.

Figure E4: **Generation of *Foxfl*^{WT/S52F} knock-in mouse.** (A) Schematic diagram shows the generation of *Foxfl*^{WT/S52F} knock-in mouse line using CRISPR/ Cas9 genome editing. (B) Nucleotide sequences of WT and S52F *Foxfl* alleles. (C) Genotyping of WT and *Foxfl*^{WT/S52F} mutant mice by PCR.

Figure E5. ***Foxfl*^{WT/S52F} mice exhibit decreased body weight after birth.** (A) Image shows sizes of E16.5 *Foxfl*^{WT/S52F} and WT embryos after dissection. (B-C) *Foxfl*^{WT/S52F} and WT embryo weights and their graphical representation show no significant differences. The number of

embryos (N) used for analysis is provided in the Table. (D-E) *Foxf1*^{WT/S52F} mice had a gradual decrease in their body weight after birth compared to WT littermates. $p < 0.05$ is *.

Figure E6: **Misalignment of veins is observed in lungs of *Foxf1*^{WT/S52F} E18.5 embryos.** Hematoxylin and eosin (H&E) staining of E18.5 lungs shows misalignment of pulmonary veins in *Foxf1*^{WT/S52F} embryos. Magnification: x200. Abbreviation: Br, bronchiole; A, artery; V, vein.

Figure E7. **Histological evaluation of *Foxf1*^{WT/S52F} mice at postnatal day 15.** H&E staining shows alveolar simplification, fibrin accumulation, arterial hypertrophy and hemorrhage in *Foxf1*^{WT/S52F} lungs. Magnification: left panels, x50; remaining panels, x400. Abbreviations: A, artery; V, vein; Br, bronchiole.

Figure E8. **Rudimentary gall bladders in *Foxf1*^{WT/S52F} mice.** (A) Rudimentary gall bladder structures were found in *Foxf1*^{WT/S52F} mice after histological evaluation. *Foxf1*^{WT/S52F} and WT mice were harvested at 8 weeks of age. Magnification: upper panels, x10; bottom panels, x50. Whole liver (B) and the gall bladders with cystic ducts (C) were dissected and photographed. Abbreviations: Li, liver; Gb, gall bladder.

Figure E9. **Loss of peripheral microvasculature in E18.5 *Foxf1*^{WT/S52F} lungs.** (A) Reduced PECAM1 and FLK1 in *Foxf1*^{WT/S52F} E18.5 lungs. *Foxf1*^{WT/S52F} and WT embryos were harvested at E18.5. Paraffin lung sections were stained with PECAM1 or FLK1 Abs (dark brown) and counterstained with nuclear fast red (red). Inserts show higher magnification images. Immunostaining for endomucin (green) was performed using postnatal day 7 (P7) lungs and show the loss of microvascular network in the peripheral lung of *Foxf1*^{WT/S52F} embryos. Slides were counterstained with DAPI. Magnification: left and middle panels, x200; inserts in left and middle panels, x400; right panels, x400; inserts in right panels, x800. (B) Decreased vascular perfusion in *Foxf1*^{WT/S52F} P2 lungs. P2 pups were I.V. injected with Isolectin B4 and 15 mins later whole mouse lungs were imaged using confocal microscopy. Reduced vascular perfusion is observed in peripheral lung regions located near pleural surface (pl). Microvasculature is present around bronchioles (br) of *Foxf1*^{WT/S52F} lungs. Red shows isolectin B4, green shows autofluorescence.

Figure E10. **S52F mutation does not change expression of epithelial and smooth muscle proteins.** (A) Immunohistochemical staining of epithelial and smooth muscle cell markers shows no differences in their expression patterns in *Foxf1*^{WT/S52F} E15.5 lungs compared to WT. (B)

qRT-PCR shows no differences in *Acta2*, *Pdpr*, *Sftpc* or *Scgbla1* mRNAs between *Foxf1*^{WT/S52F} and WT E15.5 lungs (n=3 embryos in each group). (C) Immunostaining for Lyve-1 shows the presence of lymphatic vessels in *Foxf1*^{WT/S52F} newborn lungs. H&E staining shows morphology of arteries (Ar) and veins (Ve) located near pulmonary bronchioles (Br). Magnification: upper and bottom panels in A and C, x400.

Figure 11. **Histology of the heart, kidney and intestinal tract in WT and *Foxf1*^{WT/S52F} mice.** H&E staining was used to examine histology of trachea (Tr), esophagus (Eso), left ventricle of the heart (Lv), kidney (Ki) and the distal part of intestinal tract. Mice were harvested at P2. Cart, cartilage. Magnification: panels in A, C and D, x50; panels in B, x100.

Figure E12. **FOXF1 protein binds to *Stat3* gene locus.** (A) Immunoblots show efficiency of *Foxf1* knockdown in MFLM-91U endothelial cells. FOXF1 levels were decreased by siRNA (*siFoxf1*). (B) Immunofluorescent images show decreased STAT3 staining (arrowheads) in FOXF1-depleted cells. Magnification: x400. (C) ChIP-seq shows DNA regions in mouse *Stat3* gene locus (black boxes) bound by FOXF1 and regions with positive (green) and negative (red) histone methylation marks.

Figure E13. **FOXF1 and STAT3 regulate gene expression in endothelial cells.** (A) Overexpression of *Stat3* in FOXF1-deficient endothelial cells stimulates expression of cell cycle regulatory genes *Ccnd1*, *Ccnb1* and *c-Myc*. Transfection was performed in MFLM-91U cells. mRNAs were detected by qRT-PCR and normalized to β -*actin* mRNA (n = 3 independent cell cultures in each group). (B) Overexpression of FOXF1 in STAT3-deficient MFLM-91U cells increases *Foxf1*, *Pecam1* and *Flkl* mRNAs but does not change *Ccnd1*, *Ccnb1* and *c-Myc* mRNAs. STAT3-specific siRNAs (siStat3-1 and siStat3-2) were used to inhibit *Stat3* expression (n=3 independent cell cultures in each group). The efficiency of *Stat3* inhibition is shown by Western blot (insert). Asterisk indicate p<0.05. Abbreviations: NS, not significant; CMV, cytomegalovirus promoter.

Figure E14. **FOXF1 and STAT3 cooperate to regulate gene expression.** (A) Venn diagram reveals that FOXF1 and STAT3 have a 72% overlap in downstream target genes identified by ChIP-seq. (B) Table shows the list of selected genes regulated by both FOXF1 and STAT3. Genomic location of transcriptional start site (TSS) of genes and DNA regions bound by FOXF1 and STAT3 are indicated. Overlapping binding regions are shown in red.

Figure E15. **ChIP-seq diagrams show binding regions for FOXF1 and STAT3.** Binding regions and histone methylation marks are shown in *Ccnd1*, *Mmp2*, *Pecam1*, *Cdh5*, *Bax* and *Bcl2* gene loci. Black boxes indicate active enhancer regions bound by both FOXF1 and STAT3.

Figure E16. **3D model of the forkhead DNA binding domain.** A 3D model of the forkhead domain of human FOXF1 in two projections. The domain consists of α -helices H1, H2, and H3, β -strands S1, S2, and S3, and two wings W1 and W2. (a) and (b), WT FOXF1 with S52 sidechain are rendered as a stick. (c), A zoomed-in view at S52. (d) and (e), S52F mutation with phenylalanine highlighted in red. (f), A zoomed-in view at F52. The model predicts that S52F introduces a steric hindrance and reduces binding affinity of FOXF1 to the targeted DNA binding site.

Figure E17. **Strategy for the preparation of nanoparticles.** (A) EDC/NHS based conjugation scheme. (B) PEI600-MA5.0 atr-FTIR showing amide carbonyl stretching $\nu = 1650 \text{ cm}^{-1}$ and the disappearance of carboxylic acid stretching $\nu = 1290 \text{ cm}^{-1}$ in the conjugated polymer. (C) FACS gating strategy for identification of hematopoietic (a), endothelial (b), lineage negative (c) and epithelial (d) cells in lung tissue. (D) Polyplex size and zeta potentials reported from DLS measurements in normal glucose at a w/w ratio of 24. Respective distribution of colloidal sizes from DLS.

Figure E18. **Accumulation of PEI 600-MA5.0 nanoparticles in FACS-sorted cells.** (A) Bar graph shows mean fluorescence intensity of DyLight 650 in different cell populations of WT lungs harvested 24 hr after injections of nanoparticles. Statistical significance ($p < 0.05$) was calculated using an unpaired t-test assuming unequal variance ($n = 3$ mice). (B) CMV-STAT3 and CMV-GFP were incorporated into the same nanoparticles that were injected into the facial vein of P2 mice. GFP fluorescence in $\text{CD31}^+\text{CD45}^-$ endothelial cells was measured by FACS using P5 lungs. Asterisk indicate $p < 0.05$ ($n = 3$ mice). (C) Immunostaining shows expression of GFP reporter in the lung tissue. Magnification: x200; inserts, x2000.

Figure E19. **Nanoparticle mediated delivery of CMV-STAT3 inhibits lung inflammation in *Foxf1*^{WT/S52F} lungs.** Nanoparticles/DNA complexes were injected at P2, lungs were harvested at P7. CMV-STAT3 reduces lung inflammation and improves lung structure in *Foxf1*^{WT/S52F} neonates. Magnification: upper panels, x100; bottom panels, x400.

Figure E20. **Nanoparticle STAT3 delivery does not affect histology and vasculature of the heart, liver and kidney.** H&E staining and immunostaining for endomucin (green) of frozen sections from liver, heart and kidney shows no phenotypic differences in histology and vasculature of these organs after nanoparticle-mediated delivery of CMV-STAT3. Nanoparticle/DNA complexes were injected at P2, lungs were harvested at P7. Magnification: x100.

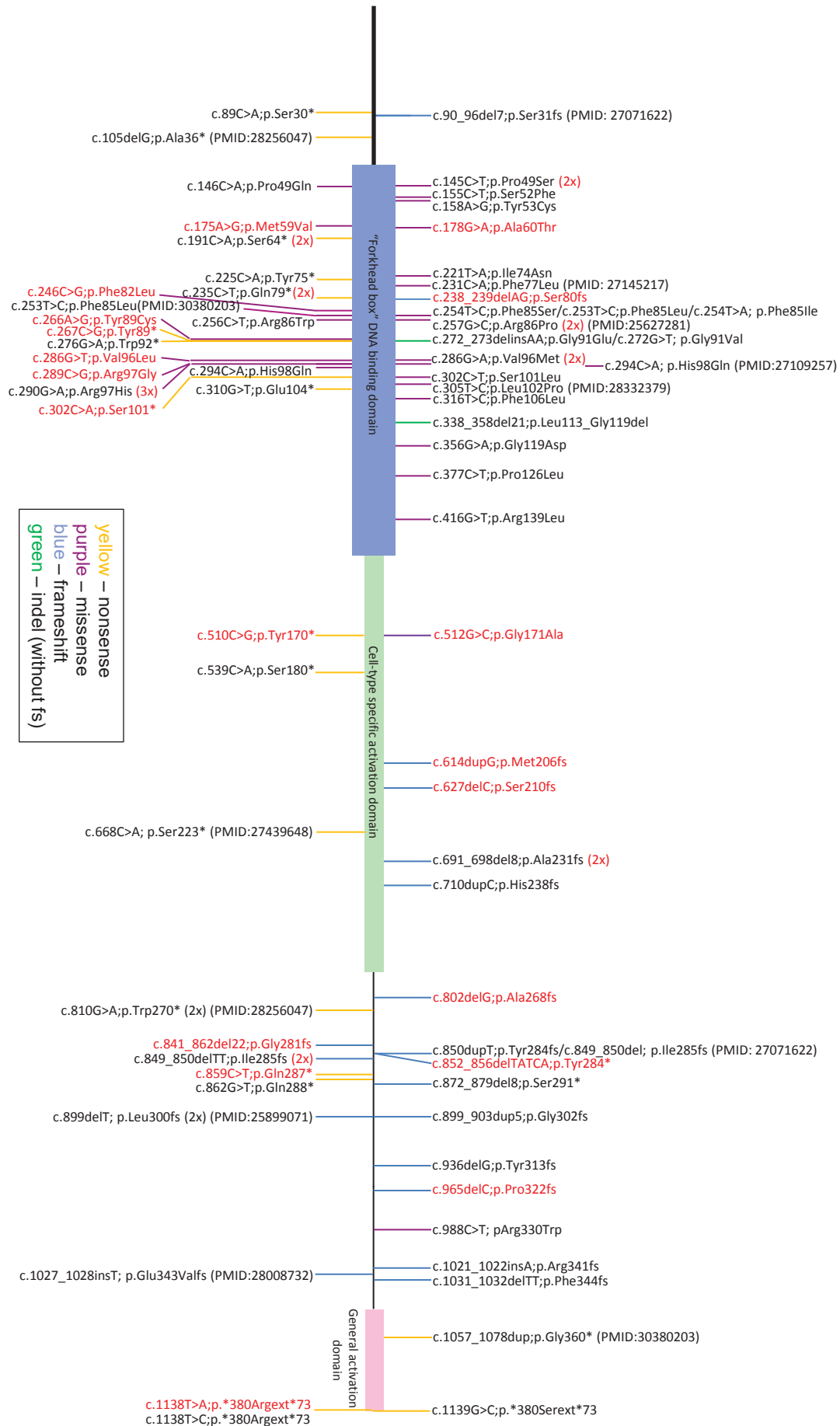


Figure E1

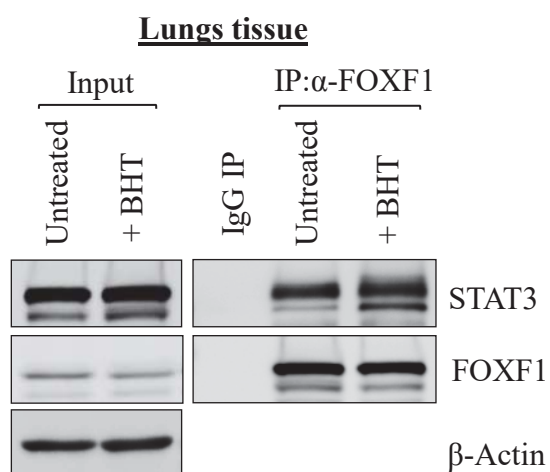
(A)

Human	TNAGIRRPEKPPYSYIALIVMAIQ
Mouse	TNAGVRRPEKPPYSYIALIVMAIQ
Chimpanzee	TNAGIRRPEKPPYSYIALIVMAIQ
Dog	TNAGFRRPEKPPYSYIALIVMAIQ
Chicken	TNAGIRRPEKPPYSYIALIVMAIQ
Frog	TNAGIRRPEKPPYSYIALIVMAIQ
Zebra fish	TNAGIRRPEKPPYSYIALIVMAIQ

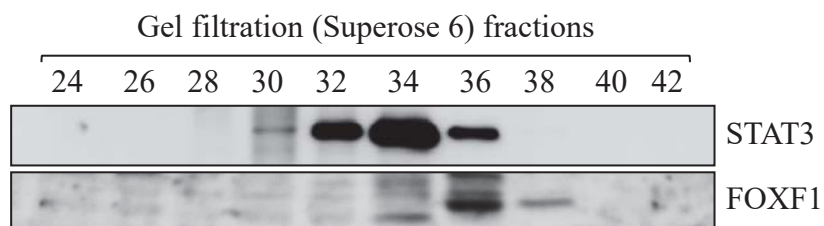
(B)

FOXF1	-KPPYSYIAL
FOXF2	-KPPYSYIAL
FOXC1	-KPPYSYIAL
FOXD1	-KPPYSYIAL
FOXM1	-RPPYSYMAM
FOXJ1	-KPPYSYATL
FOXA2	-KPPYSYISL

(C)



(D)



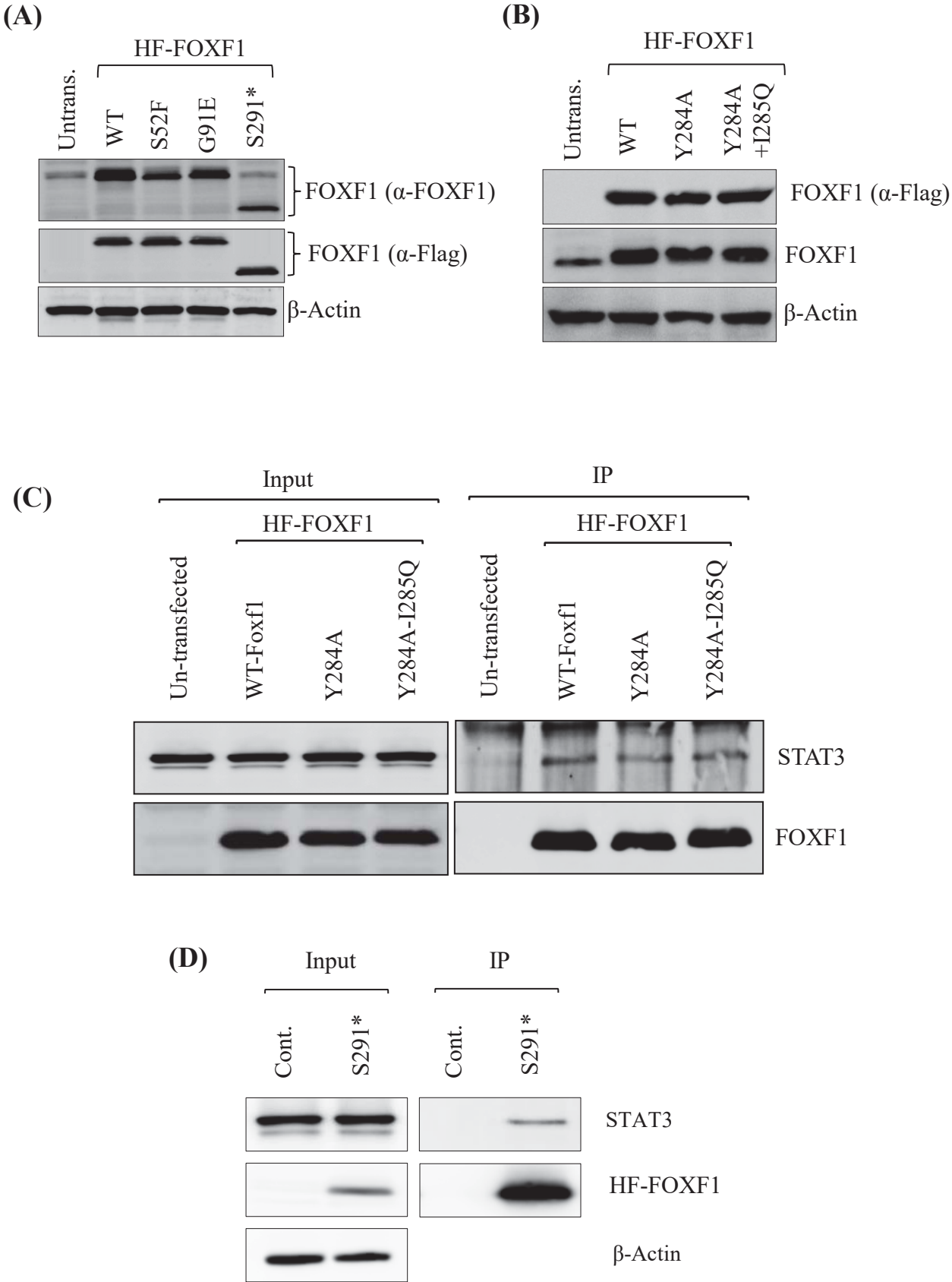
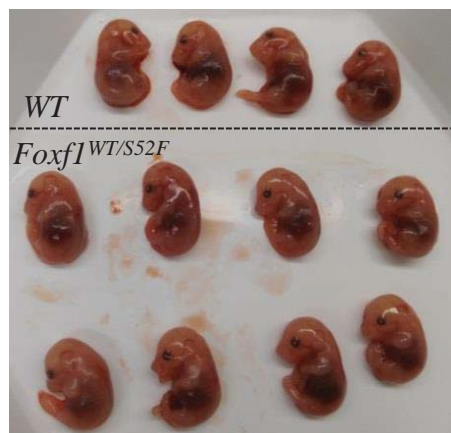


Figure E5

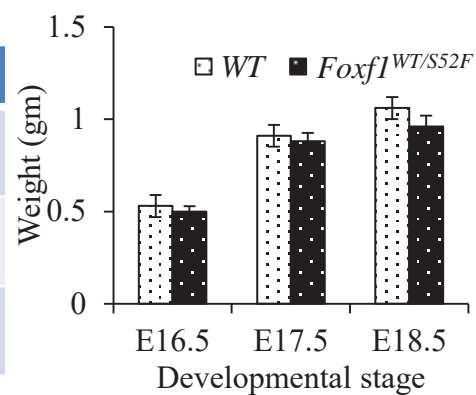
(A)



(B)

Stage	WT	<i>Foxf1</i> ^{WT/S52F}
16.5E	0.53g (N=15)	0.50g (N=12)
17.5E	0.91g (N=11)	0.88g (N=4)
18.5E	1.06g (N=22)	0.96g (N=11)

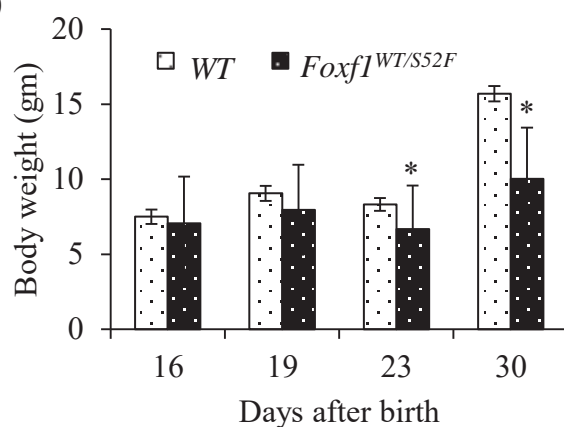
(C)



(D)

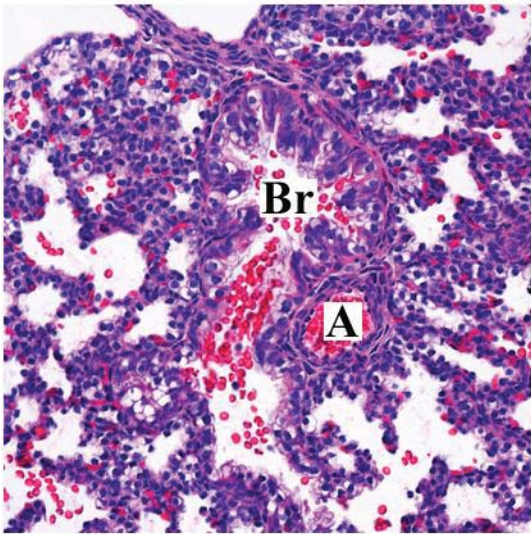
Days	WT	<i>Foxf1</i> ^{WT/S52F}
16	7.51g (N=8)	7.07g (N=12)
19	9.06g (N=20)	7.97g (N=10)
23	8.32g (N=22)	6.68g (N=17)
30	15.7g (N=4)	10.02g (N=4)

(E)



E18.5 Embryos

WT



Foxf1^{WT/S52F}

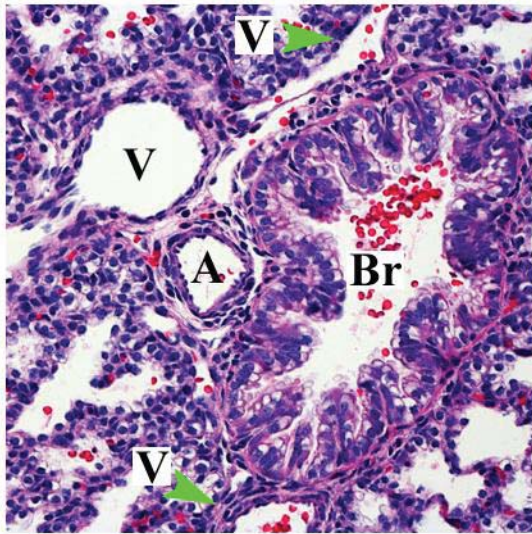


Figure E7

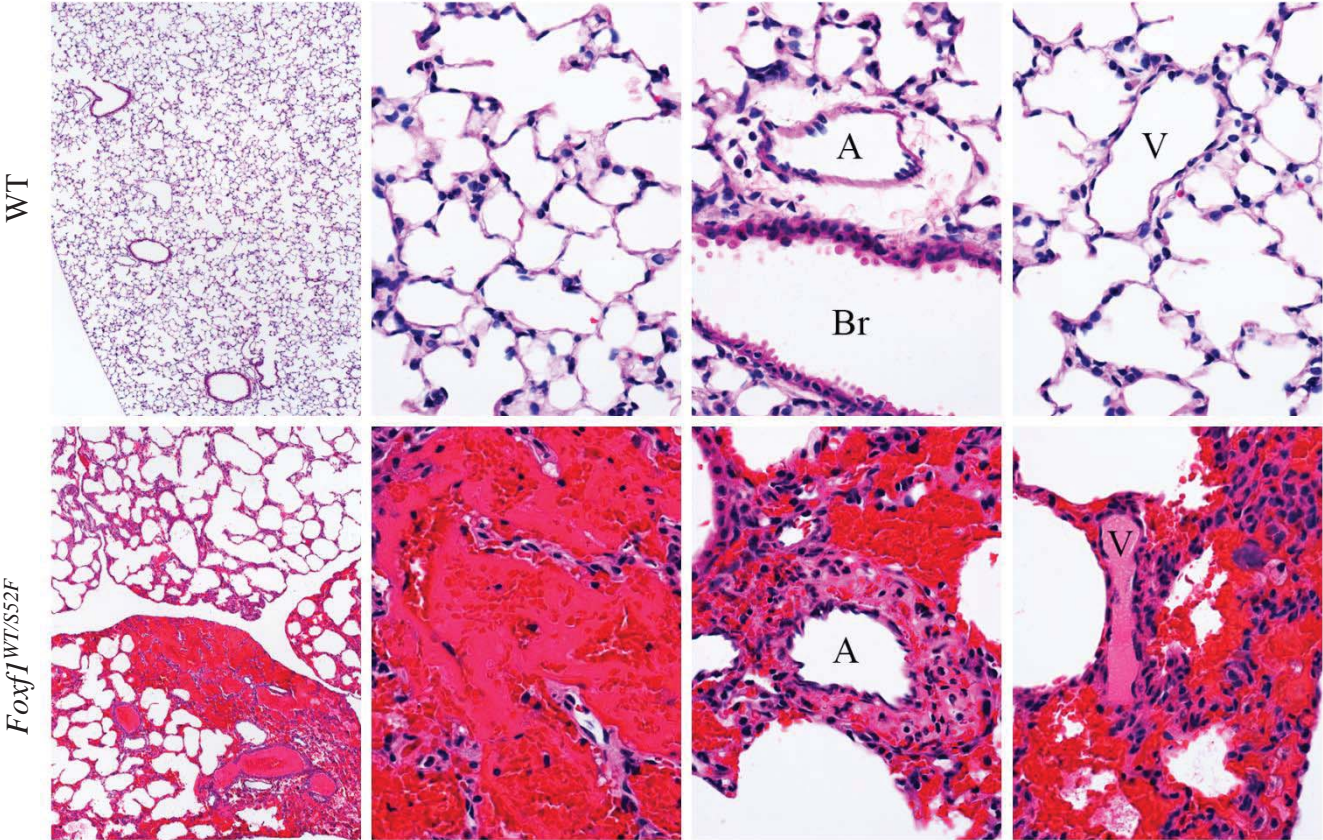
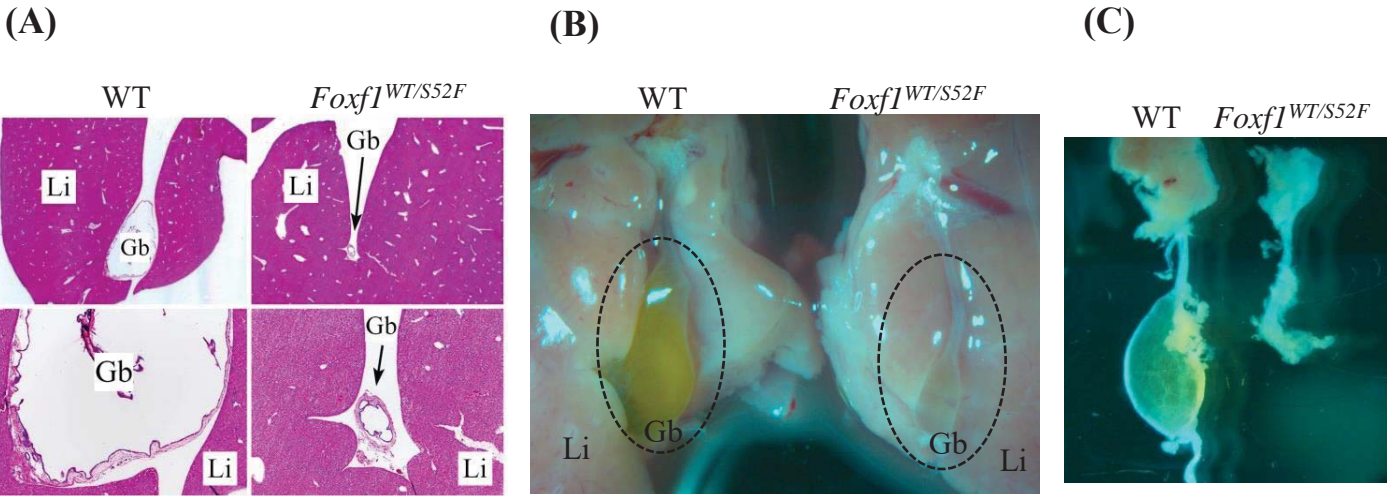
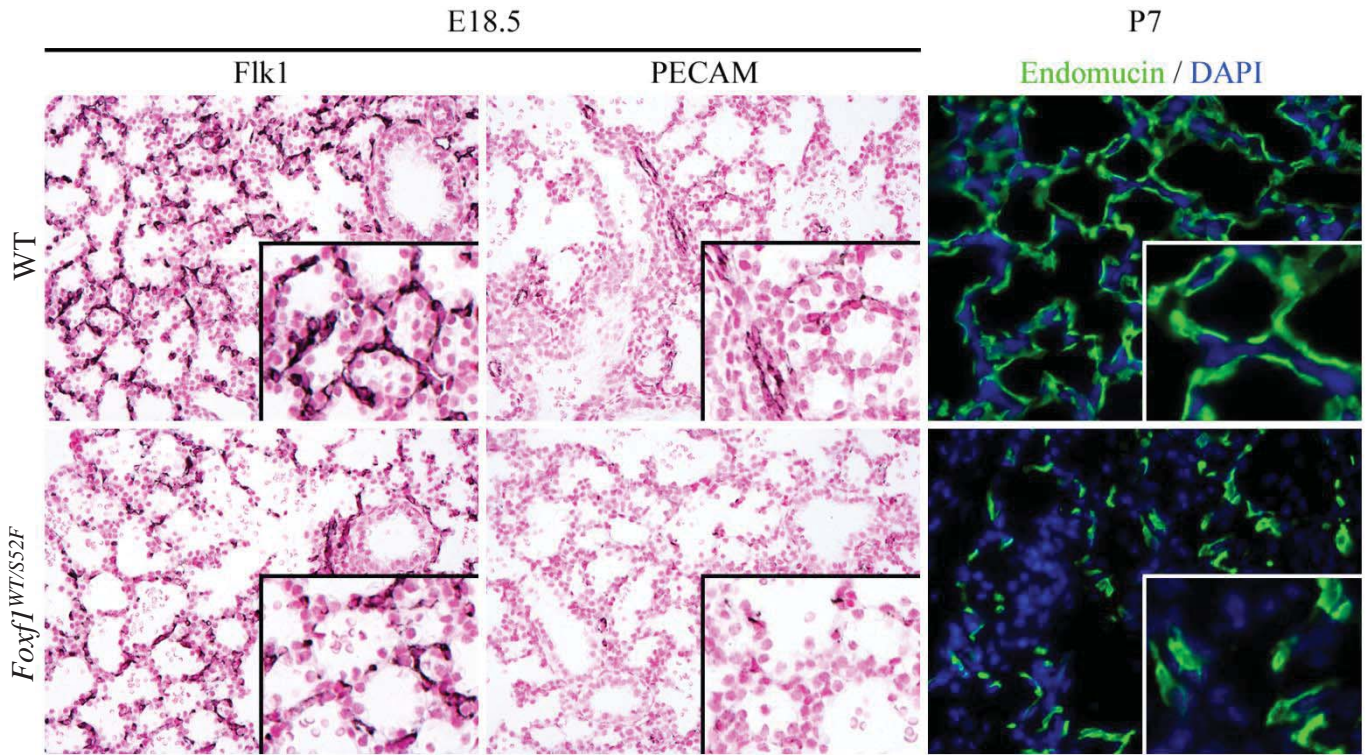


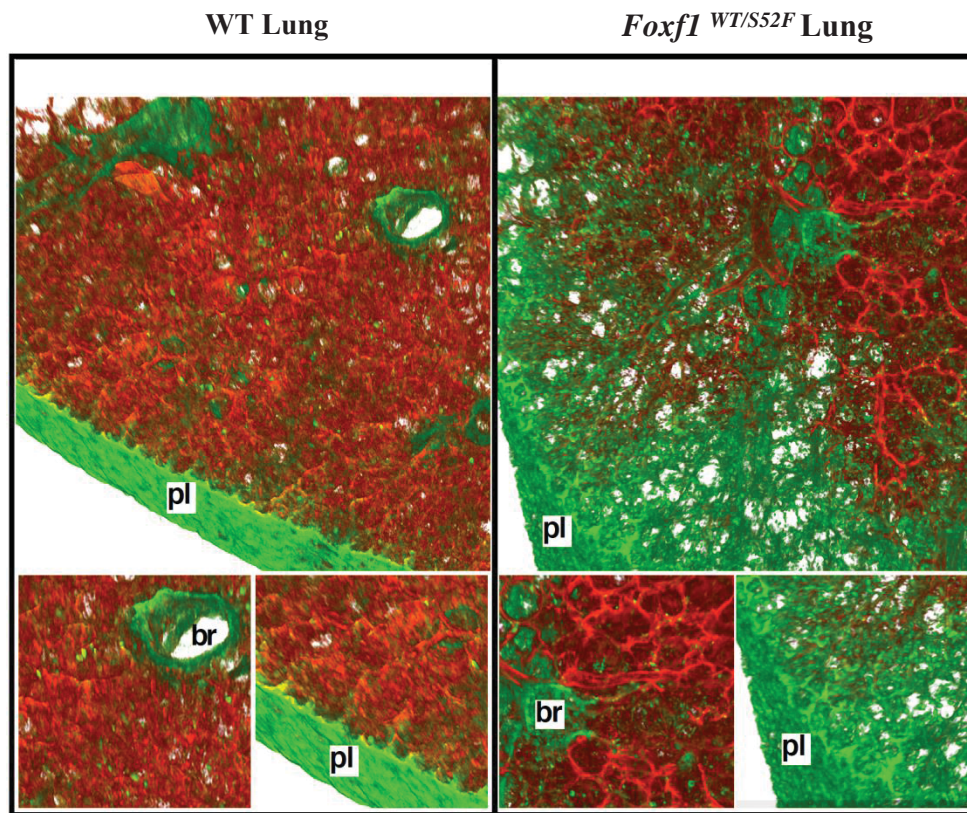
Figure E8

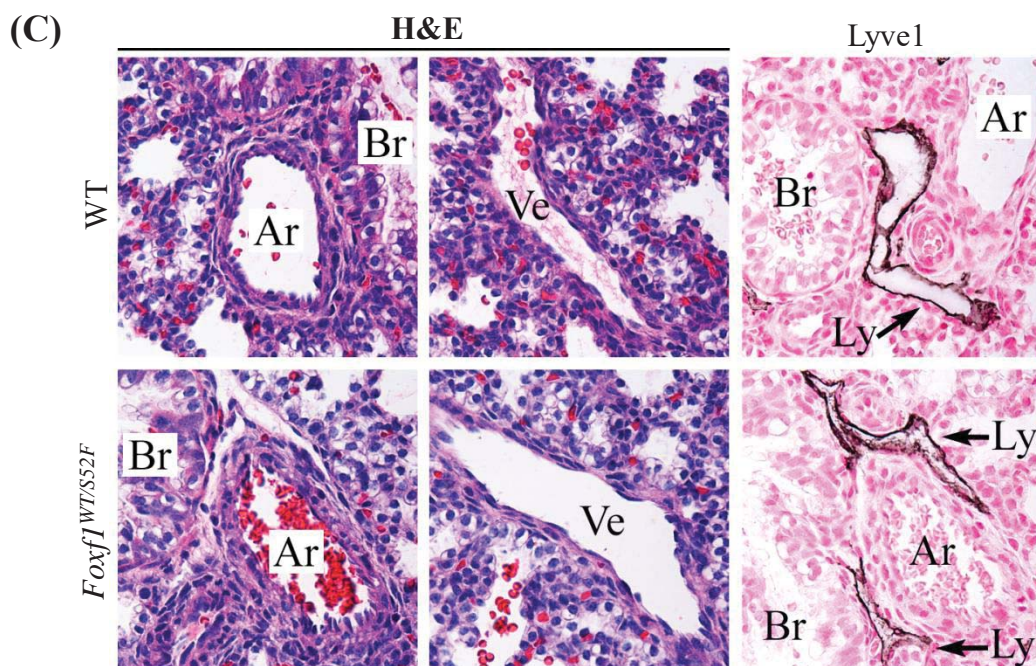
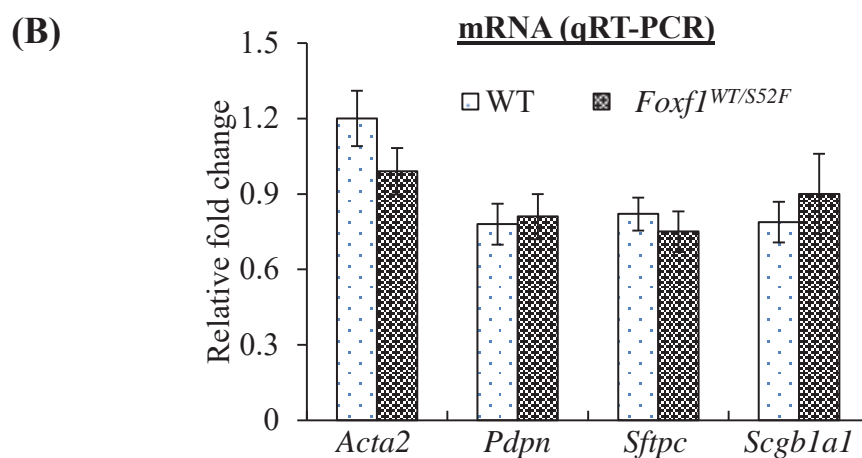
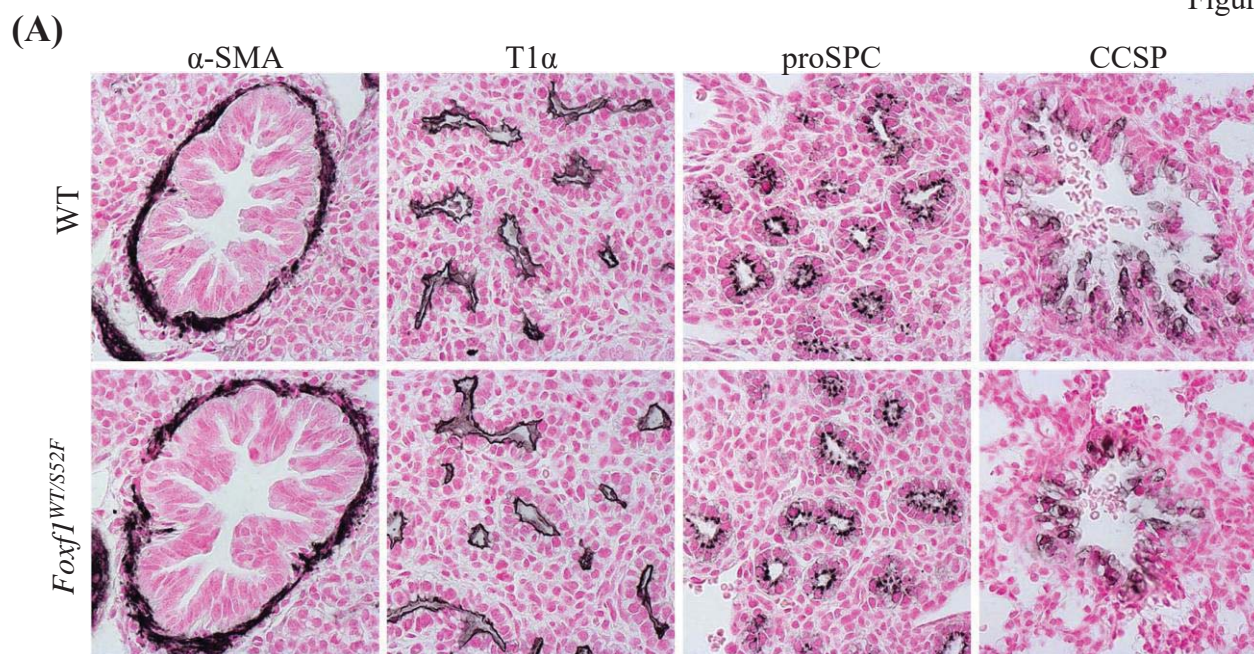


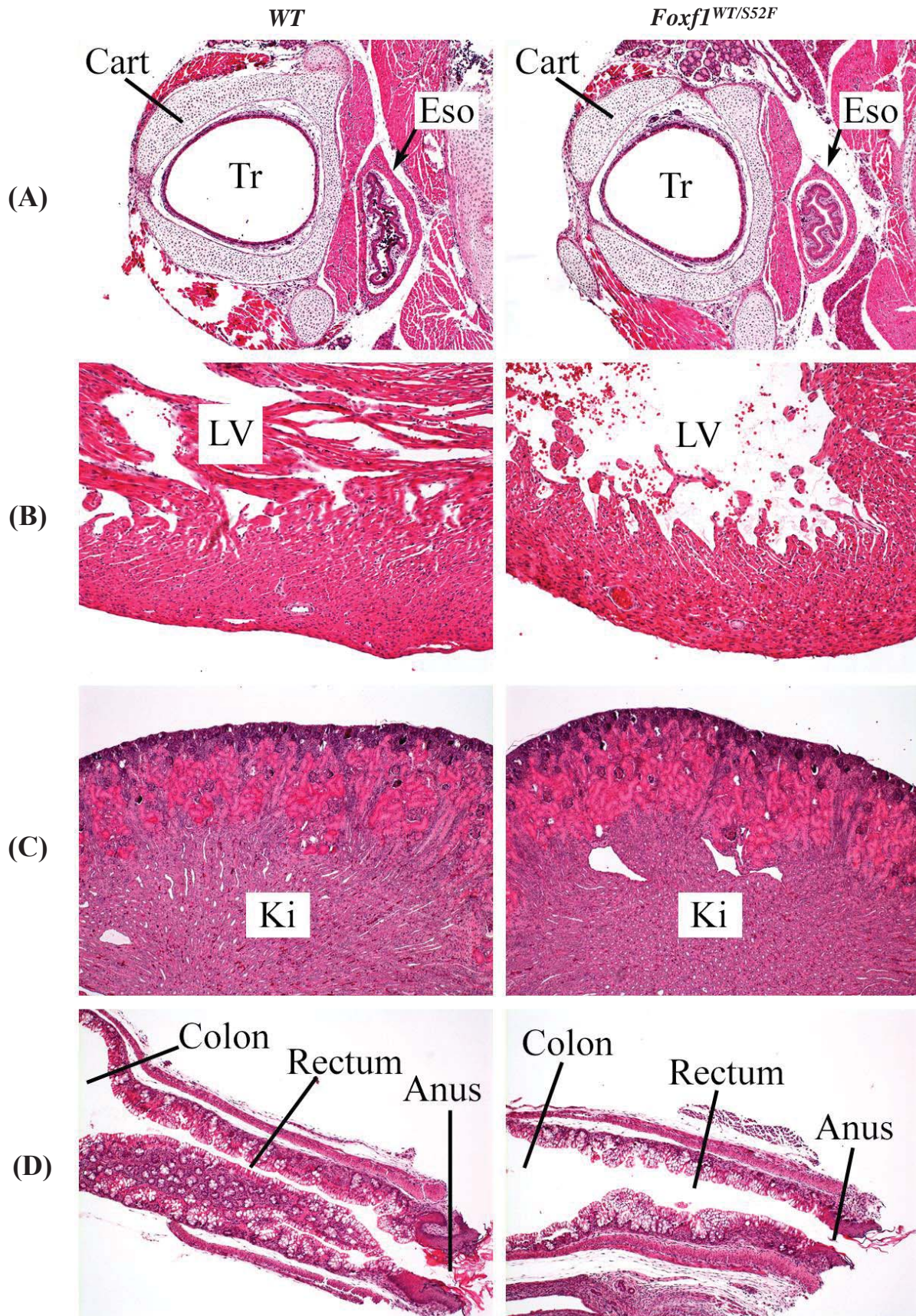
(A)

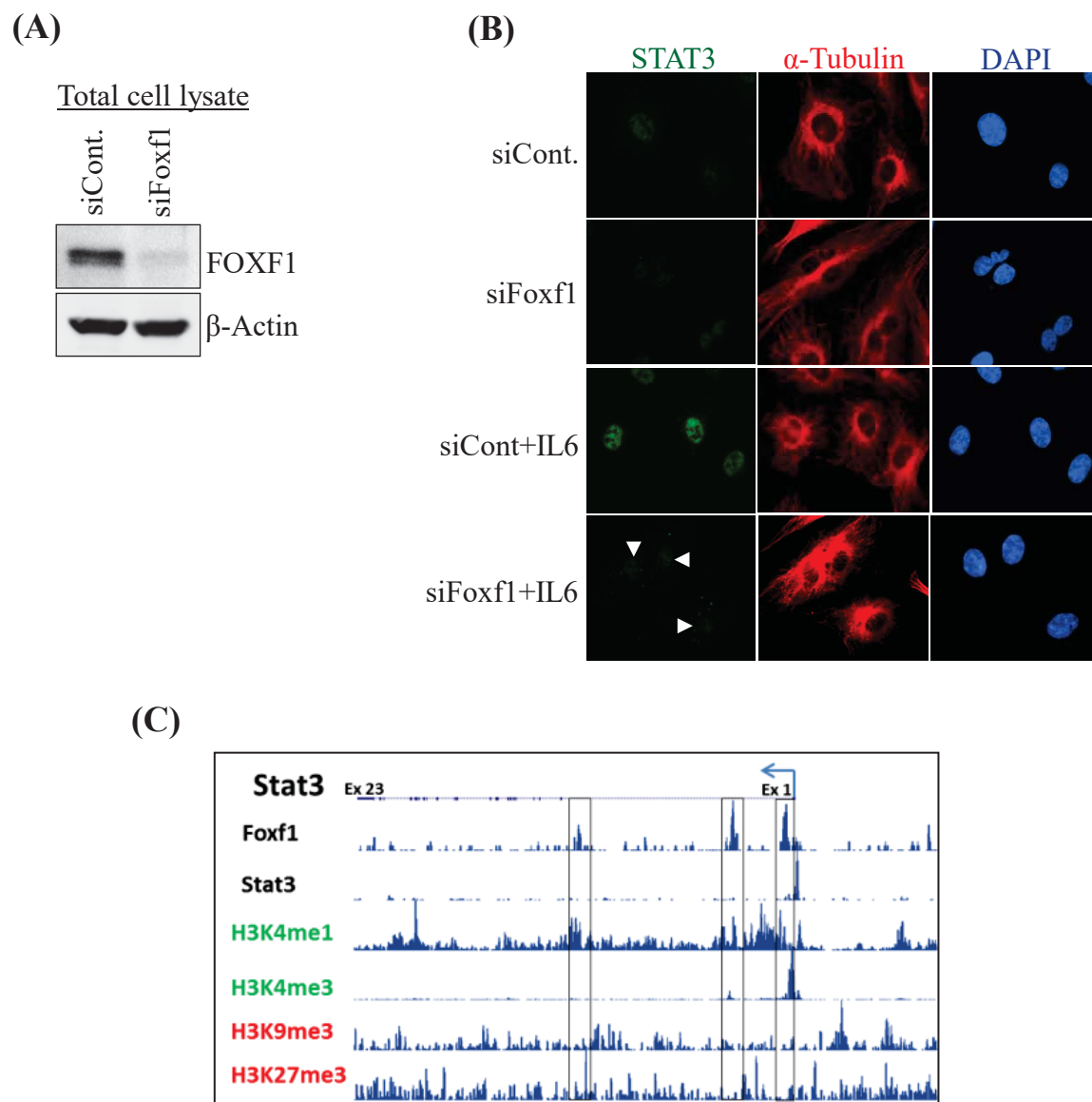


(B)

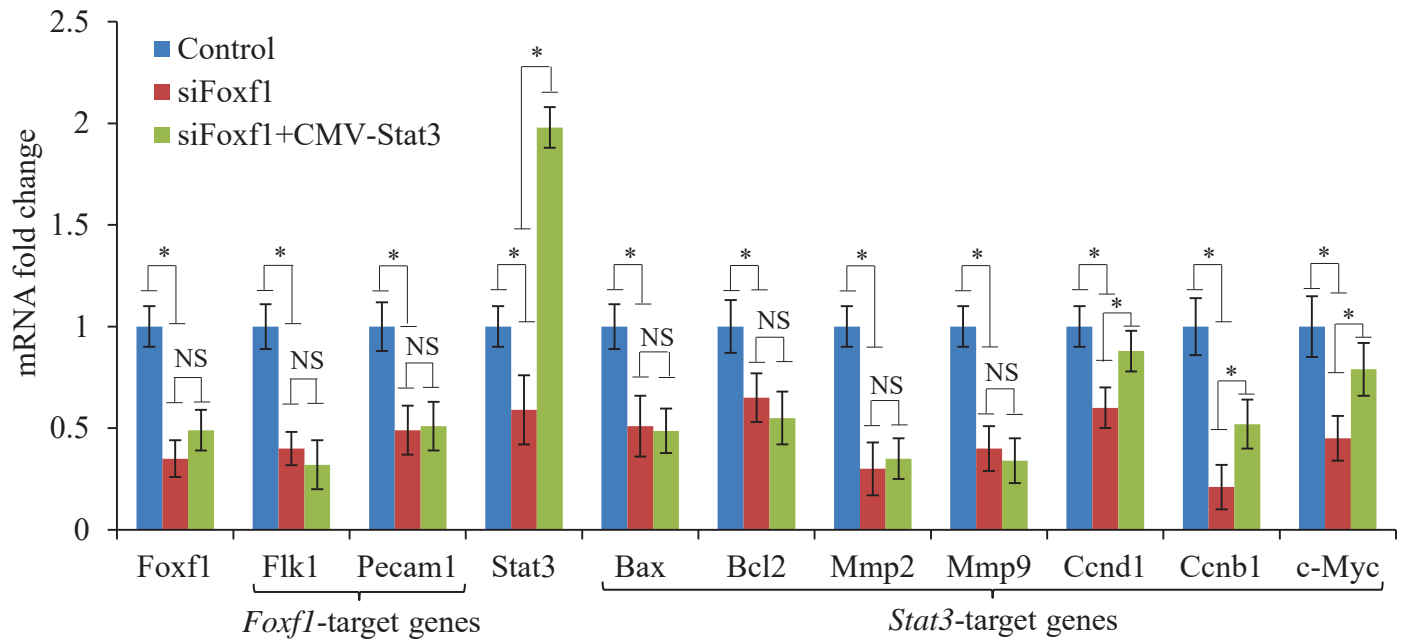




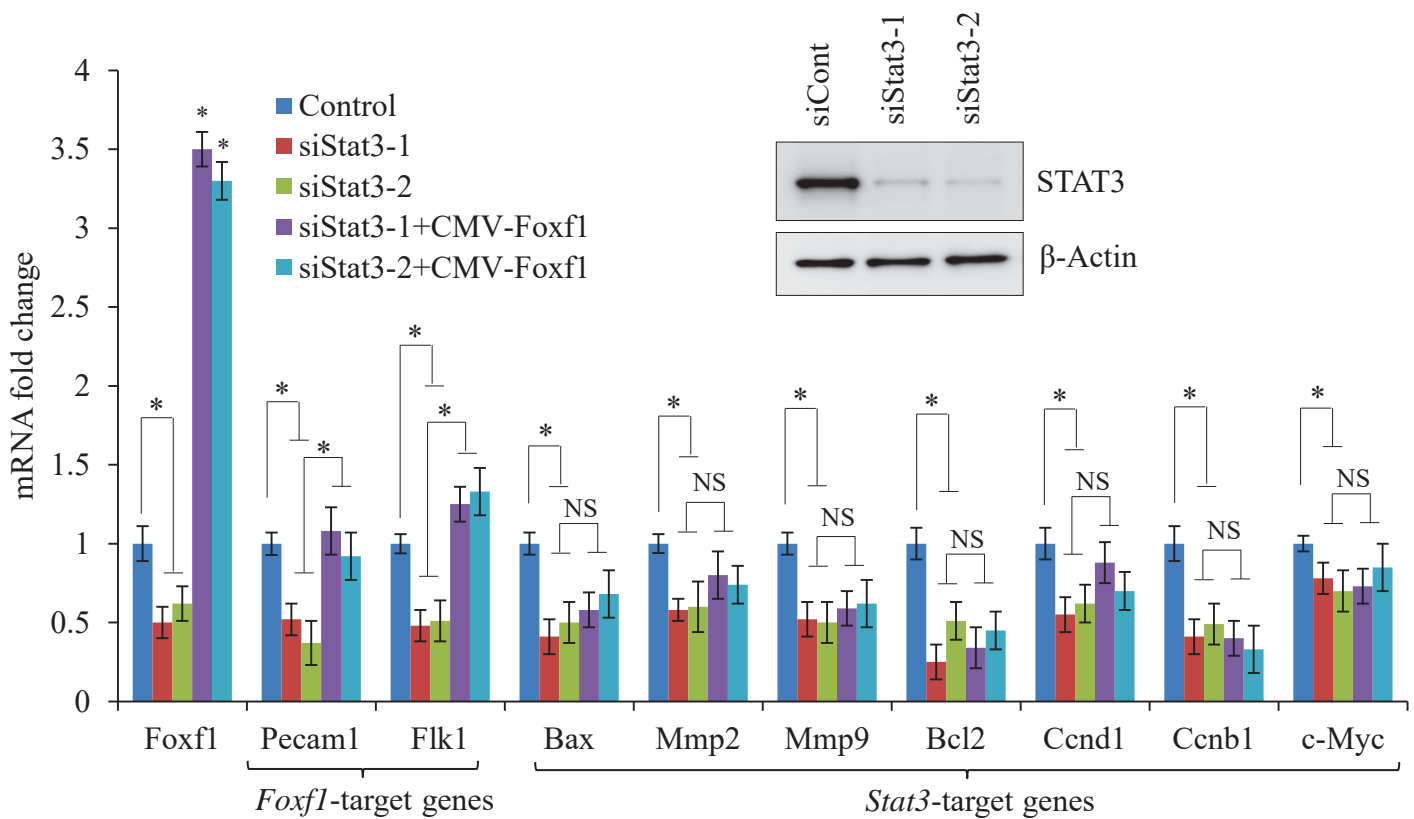




(A)



(B)



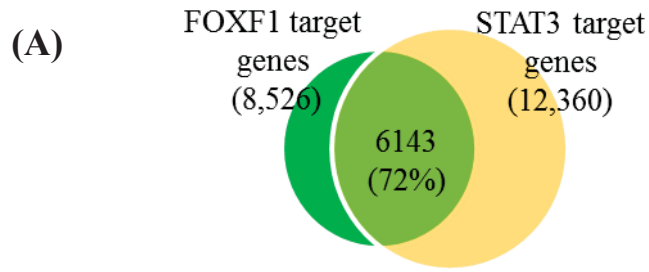
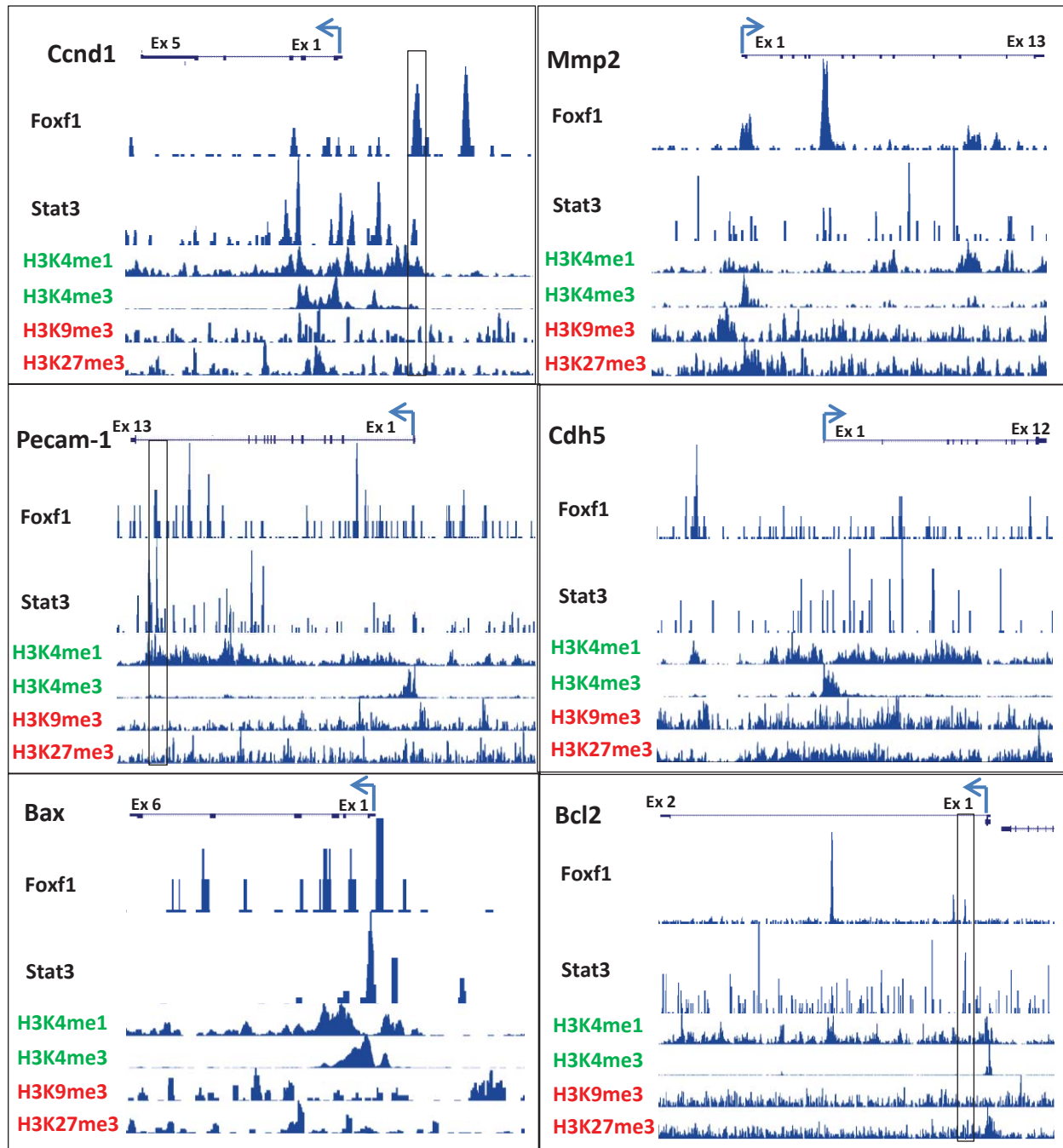


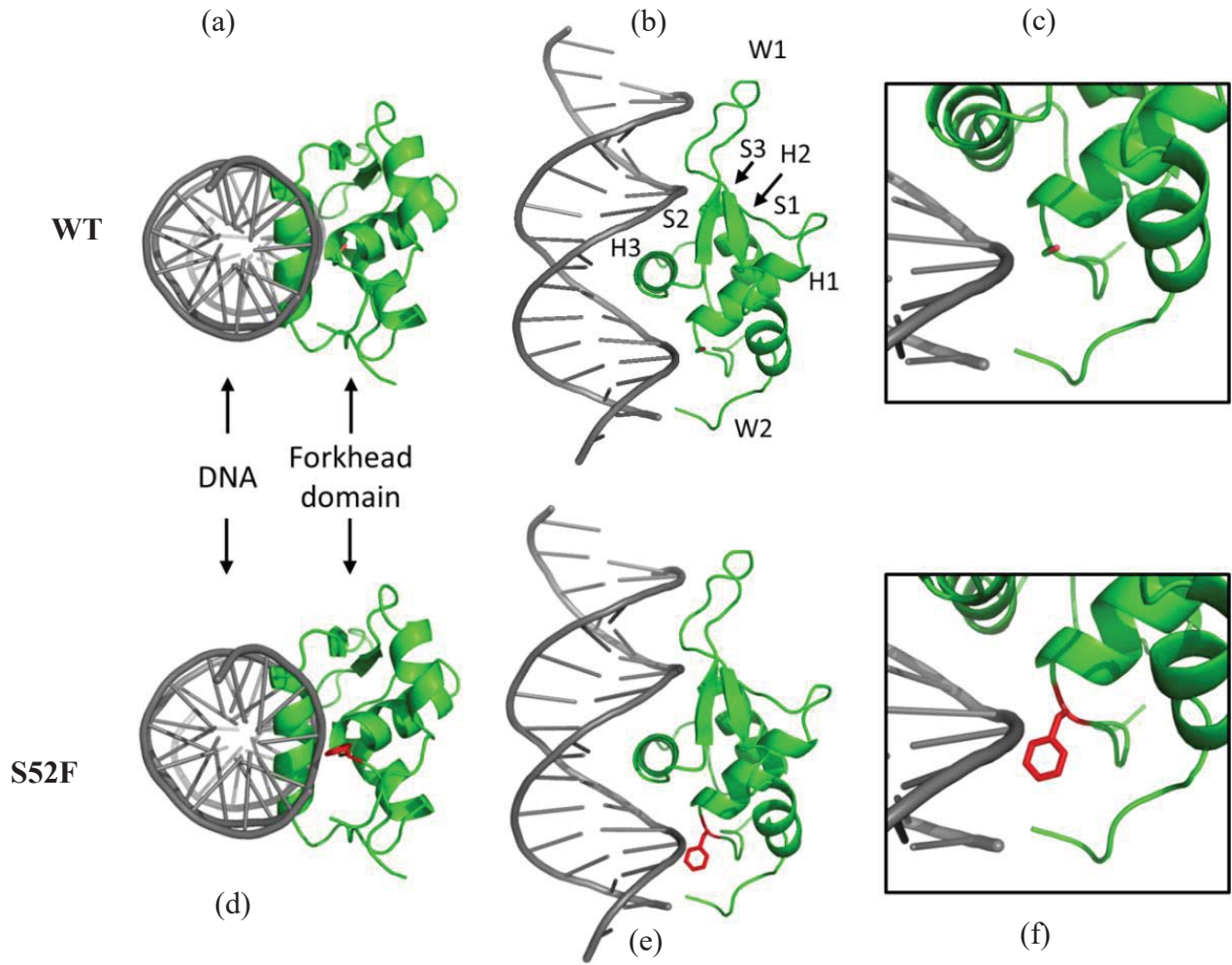
Figure E14

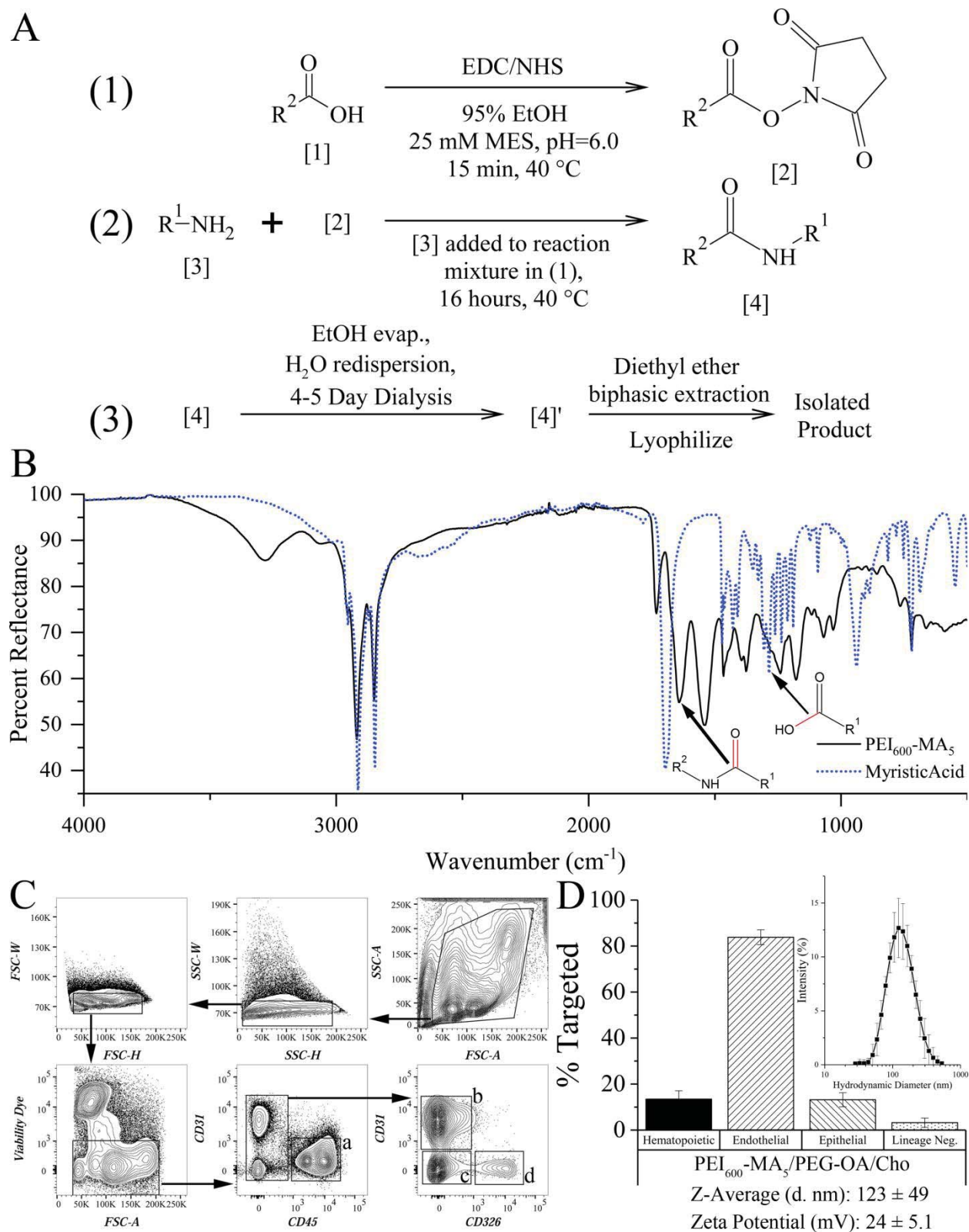
(B)

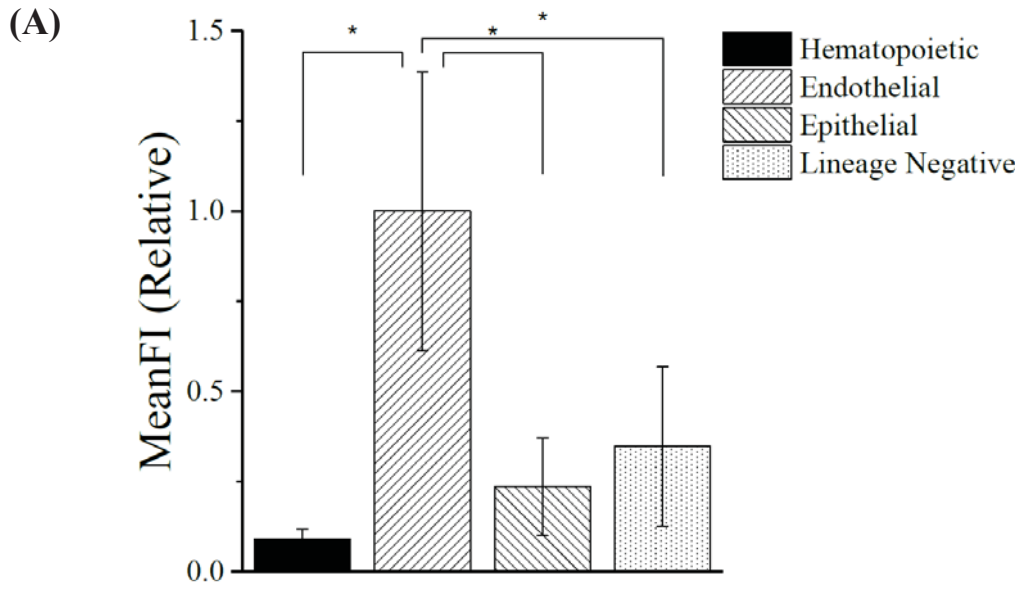
	Chromosome	TSS	FOXF1		STAT3	
Brd4	17	32,284,133	1,018	424	-475	-760
Ccnc	4	21,727,701	2	145	-148	137
Ccnd3	17	47,505,050	-971	-108		
			-3,282	-2,885	-2,637	-2,425
			-1,862	-1,690	-126	227
			-270	600	2,885	3,296
			2,958	3,151	6,203	6,308
Ccne2	4	11,191,350	3,374	3,539	6,702	6,902
			5,782	6,660		
Ccnf	17	24,251,409	-424	287	-633	-486
Cdc45	16	18,811,973			343	478
			1,382	1,144	-102	-392
c-Myc	15	61,985,340			147	-22
			440	-62	-350	-456
Nek7	1	138,619,696			154	529
			-1,524	-1,317	-2,082	-1,536
			-961	-71	-1,003	-750
Nek9	12	85,339,362			-389	-78
					15	328
Cnd1	7	144,939,925	-356	724	-629	-454
			834	1,052	-170	627
					1,343	1,739
			-1,854	-1,997	55	-266
			2,304	1,481		
Mmp2	8	92,827,327	-5,962	-6,301	-3,413	-3,607
			-3,504	-3,881	-2,259	-2,364
					-1,569	-1,903
					-378	-552
					235	6
					613	503
Pecam1	11	106,715,281			2,274	2,095
					2,854	2,666
			-123	890	2259	2364
			6,799	7,959		
Bcl2	1	106,714,290	19,454	20,589		
			21,740	22,298		
			12,605	12,422	35,301	35,016
			48,504	48,351	39,741	39,637
			55,814	55,548	40,512	40,401
Ptprc	1	138,175,305			55,223	55,118
					55,552	55,371
Bax	7	45,466,899			57,227	56,909
Bcl2	1	106,714,290	-5,072	-5,257	1	-104
					188	39
					6,040	5,888
Bcl2	1	106,714,290	13,953	13,330	13,489	13,358
			19,999	19,490		
			85,419	83,880		

Figure E15

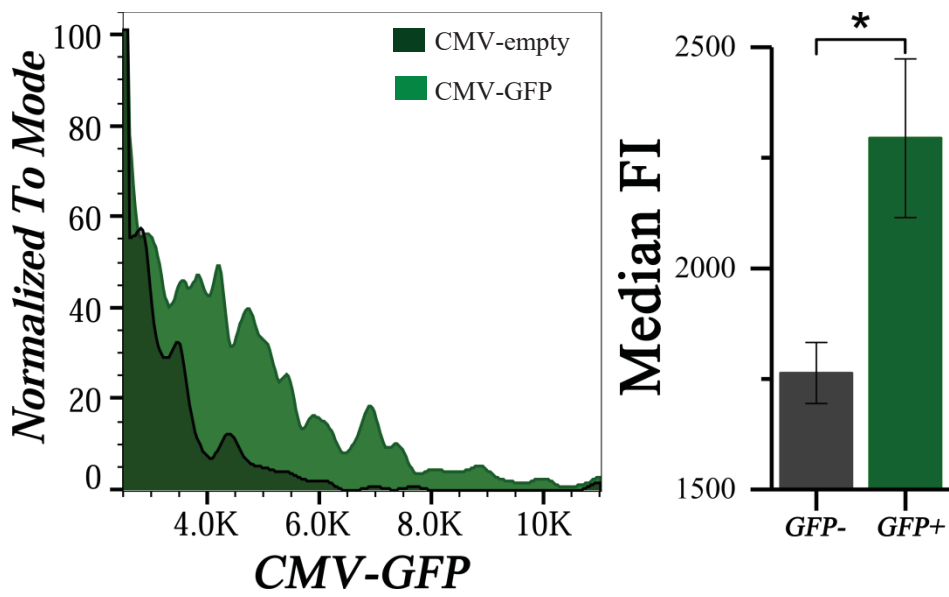




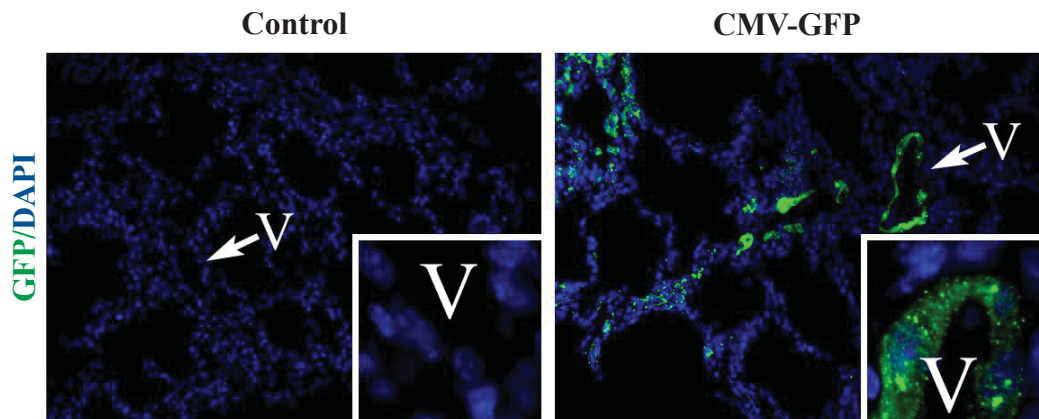




(B) Gated on endothelial cells (CD31⁺CD45⁻)



(C)



(A)

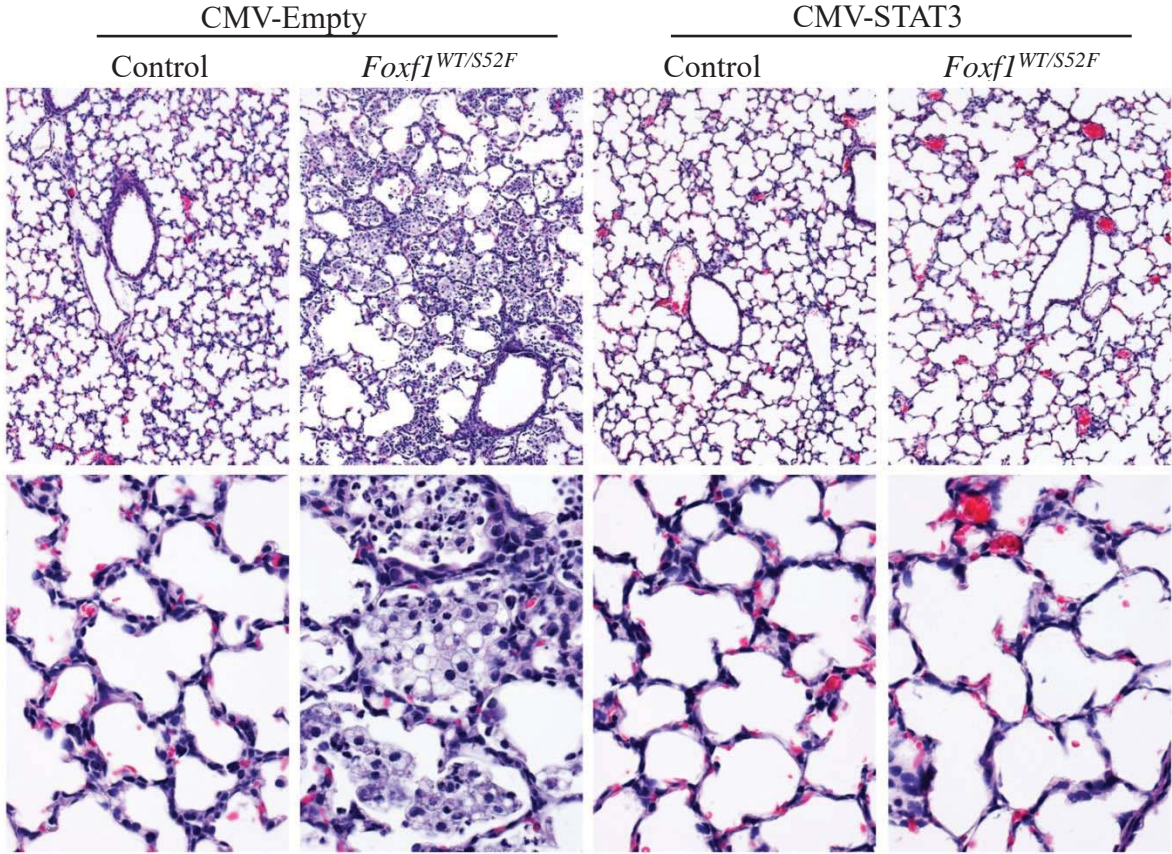


Figure E20

